Exciton binding energy and the origin of yellow-light emission in $CH_3NH_3PbBr_3$ single crystals

I. V. Zhevstovskikh [1,2] N. S. Averkiev [3,*] M. N. Sarychev [2] O. I. Semenova [4] and O. E. Tereshchenko [4]

[1]*M.N. Miheev Institute of Metal Physics of Ural Branch of RAS, Ekaterinburg 620137, Russia*

[2]*Ural Federal University, Ekaterinburg 620002, Russia*

[3]*Ioffe Institute, St. Petersburg 194021, Russia*

[4]*A.V. Rzhanov Institute of Semiconductor Physics, Siberian Branch of Russian Academy of Sciences, Novosibirsk 630090, Russia*

(Received 14 September 2023; revised 11 January 2024; accepted 1 March 2024; published 18 March 2024)

Organic-inorganic lead halide perovskites have emerged in recent years as semiconductor materials for various optoelectronic and photovoltaic applications. The exciton binding energy is an important parameter because the formation of excitons can potentially hamper charge separation in solar cells. However, it remains a challenge to experimentally determine the exciton binding energy in hybrid bromine-based perovskites: the obtained values have a tens meV spread. Here we present in detail the near-band edge photoluminescence study in $CH_3NH_3PbBr_3$ single crystals under different photoluminescence excitation densities with a 405 nm laser diode. We show that by using high laser excitation intensities it is possible to make a direct measurement of the exciton binding energy, which we find to be only 12 meV at low temperatures, lower than has been previously determined. In the low temperature orthorhombic phase, besides the free exciton emission at 2.25 eV, we observed the broad yellow-light emission at 2.16 eV, which exhibited a red shift with the increasing temperature and a blue shift with increasing laser excitation intensity. Based on the excitation power density and temperature dependence of the photoluminescence spectra, we interpreted yellow-light emission as a recombination of bound excitons and a donor-acceptor pair transition. The results obtained are essential for a better understanding of the electronic properties of these materials and provide a guideline for their further applications with improved performance.

DOI: 10.1103/PhysRevMaterials.8.034601

I. INTRODUCTION

In the past few years great attention is paid to hybrid (organic-inorganic) lead halide perovskites due to their photovoltaic performance with a rapid increase in power conversion efficiency from 3.8% [1] to 23% [2] and properties such as low exciton binding energy, long diffusion length of charge carriers, and long recombination times [3–6] suitable for potential use in optoelectronics. Among the family of hybrid lead halide perovskites, methylammonium lead bromide ($CH_3NH_3PbBr_3$) single crystals have demonstrated their practical use in the fabrication of radiation detectors, photodetectors and efficient single-color light emitting devices [7]. The study of electronic excitations near the optical band edge is crucial for hybrid perovskites since the photoexcitation states near the band gap affect the processes of charge transport and light emission in optoelectronic devices. There are two kinds of photoexcitations near the band edge of direct bandgap semiconductors: free carriers and excitons. The exciton binding energy (E_b) determines the balance of the populations between the two species [8]. Values of E_b reported in the literature for $CH_3NH_3PbBr_3$ ($MAPbBr_3$) single crystals cover a wide range from 15 to 84 meV [9–17]. Such large variations in exciton binding energies raise the question of whether free carriers or excitons are generated upon photoexcitation. Knowledge of the true exciton binding energy is also crucial for interpreting, for example, the dielectric and optical properties of lead halide perovskites. Currently, optical (absorption, reflection, ultrafast THz spectroscopy) and magnetooptical techniques are considered to be the most powerful methods to prove exciton states and determine the exciton binding energy. However, these methods are based on using equations that include parameters obtained in other experiments (such as the reduced effective mass of exciton, the dielectric constant) and some model assumptions and fittings. In addition, the magnetooptical experiment requires high magnetic fields. A simpler technique to estimate E_b is based on the temperature quenching of the photoluminescence (PL) intensity, assuming that the rate of nonradiative recombination is related only to the thermally activated exciton dissociation. The value of the E_b obtained by this method ranges from 40 to 84 meV [14,15], indicating that the assumption of a single thermally activated exciton dissociation is an unacceptable simplification. Besides, the presence of shallow defects and trap states in hybrid perovskites also affects the carrier recombination dynamics, since they have their own PL temperature dependence.

In this work, we use temperature and laser power dependent photoluminescence measurements to study the electronic excitations near the optical band edge and to determine the exciton binding energy in $CH_3NH_3PbBr_3$ single crystals. In the low-temperature orthorhombic phase in the range of 6–40 K we found the free exciton emission at 2.25 eV and a broad yellow-light emission around the value of 2.16 eV, which blue shifted with increasing of laser power density from

*averkiev@les.ioffe.ru

0.014 mW/cm^2 up to 940 mW/cm^2. The close position of a yellow-light emission to the exciton line in the PL spectrum, leading to a strong overlap of these bands, determined the motivation to study the nature of the yellow-emission band in this perovskite. If the external parameters (temperature or excitation laser power) are changed, the overlap of these PL bands may become even more pronounced and not allow a clear interpretation of the PL data with respect to the exciton. Therefore, a detailed study of the behavior of the yellow PL band as a function of temperature and laser power density was required. From the analysis of the laser power dependent intensity and peak position of the yellow-light PL emission, we attributed this emission to a bound exciton and donor-acceptor pair recombination. At higher laser power intensity (1920 mW/cm^2), the resolved hydrogenlike Wannier-Mott transitions with a small binding energy of 12 meV and a Bohr radius of 5.22 nm are detected in the PL spectra. A direct measurement of the exciton binding energy in bromide-based hybrid perovskites is essential for a better understanding of their electronic properties and for the future development of this class of materials.

II. EXPERIMENTAL METHODS

The $CH_3NH_3PbBr_3$ ($MAPbBr_3$) single crystals were synthesized by using a slow cooling temperature solution growth method, which is a versatile method for obtaining single crystals, because in this method, the saturated precursor solution shows decreased solubility when the temperature is decreased [18,19]. First, CH_3NH_3Br was synthesized by mixing 0.04 mol CH_3NH_2 (methylamine, 40 wt% aq. solution) and 0.04 mol HBr, (hydrobromic acid, 46wt% in water) in a molar ratio of CH_3NH_2: HBr=1:1 at 0° C for 2 h. Then 0.04 mol $PbBr_2$ was added and dissolved in a HBr, resulting in a solution of $CH_3NH_3PbBr_3$. As an improved technique, seed assisted growth is often used to grow large-sized single crystals. To do this, small crystals were added to a solution saturated at 65° C, followed by the temperature-lowering process. The solution was gradually saturated by decreasing the temperature at a rate of 0.15° per hour from 65° C to room temperature, resulting in the formation of large, transparent, orange, high quality single crystals over the following 12 days. The grown crystals were then removed from the solution, washed with ether, and dried. As a result, we obtained bulk single crystals with typical dimensions of 2×3×5 mm^3.

The lattice parameter, unit cell volume, and phase of $CH_3NH_3PbBr_3$ single crystals at room temperature were determined by high resolution x-ray diffractometer (XtaLAB Synergy, Dualflex, HyPix, Rigaku Oxford diffraction) using Mo Kα radiation of wavelength $\lambda = 0.71073$ Å. We have verified that at room temperature the unit cell of $CH_3NH_3PbBr_3$ has *Pm-3m* cubic symmetry with the lattice parameters a=b=c=5.92770(10) Å and volume V= 208.285(11) Å^3 (final R indexes $R_1 = 3.88\%$, $wR_2 = 10.22\%$), which is in agreement with the previously reported data [20,21].

The low temperature photoluminescence (PL) spectra were obtained by mounting the sample on a closed cycle helium cryostat (Janis CCS-150) under a vacuum. The sample was excited with a 405 nm CW laser diode at 300 mW power; the laser spot size on the sample was about 2 mm^2. Using several filters to reduce the laser power density, we changed its value from 0.014 mW/cm^2 up to 1920 mW/cm^2, and the temperature varied from 6 K up to 140 K with 5 K increments. The PL spectra in the wavelength range of 500–750 nm were recorded using an MDR-23 monochromator with an InGaAs photodiode detector.

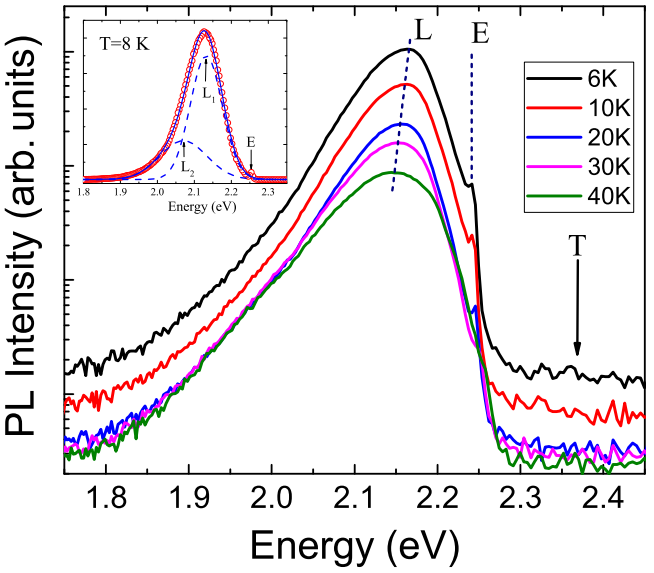

FIG. 1. PL spectra of $MAPbBr_3$ single crystals at different temperatures ($\lambda_{exc} = 405$ nm). Inset: the PL spectrum at $T = 8$ K, dashed lines show a fitting with two Gaussian peaks.

III. RESULTS AND DISCUSSION

The results of the temperature and laser excitation dependent photoluminescence (PL) spectra of the $MAPbBr_3$ single crystal are presented in Figs. 1 and 2. We found a narrow PL line at 2.252 eV (marked as E) and a broad yellow-light

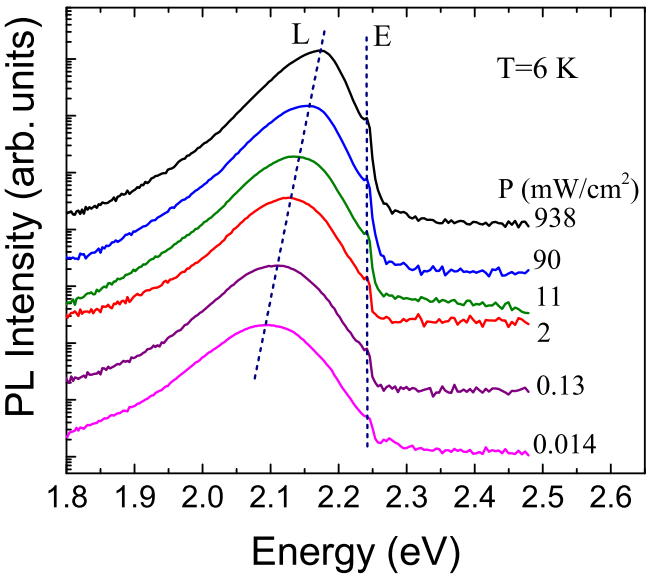

FIG. 2. PL spectra of $MAPbBr_3$ single crystals as a function of energy at $T = 6$ K, recorded for different laser excitation intensities.

PL emission (L band) near the value of 2.16 eV. The peak position of the E band is close to the band gap value of 2.258–2.292 eV of the perovskite $MAPbBr_3$ determined by optical and magneto absorption spectroscopy [11–13,16]. It should be noted that narrow PL emissions near the bandgap in inorganic semiconductors are often associated with the manifestation of free excitons or a shallow impurity bound exciton [22,23]. To correctly determine the origin of a narrow PL line, its energy position can be compared with the position of the free excitonic line in the optical absorption spectrum, as has been done for another organic-inorganic semiconductor [24]. In Ref. [12] the optical absorption spectrum of $MAPbBr_3$ at 5 K shows a sharp excitonic line at 2.258 eV, which is close in value to the E line at 2.252 eV. However, the small difference (6 meV) in these peak energies does not exclude the presence of a shallow impurity bound exciton. Our measurements of the PL intensity of the E peak at laser power densities ranging from 0.01 to 1000 mW/cm^2 showed that the peak intensity increases almost linearly [Fig. 5(b)]. This is typical for a free exciton, which it is difficult to saturate, but not for a bound one [25]. Increasing the laser power above 1000 mW/cm^2 may not lead to photodegradation of the $CH_3NH_3PbBr_3$ sample, similar to the $CH_3NH_3PbI_3$ perovskite [26], but in this case the application of the theory [25] developed for smaller changes in excitation laser power is not fully justified. Thus, we suggest that the similar values of the exciton peak positions in the absorption and photoluminescence spectra and the lack of tendency to deviate from the linear dependence of the E line intensity over a wide range of laser power are good arguments for the assignment of the E peak to the free exciton.

Gaussian deconvolution of the temperature-dependent PL spectra showed that the line shape of the L band can be better approximated by two peaks (see inset in Fig. 1), which we denoted as L_1 and L_2 lines. The maximum of the L band gradually shifts to lower energy with increasing temperature (Fig. 1). Another trend of the $MAPbBr_3$ PL properties is the excitation power dependence: the yellow-light emission maximum shifts to the blue range with increasing the laser excitation intensity (Fig. 2). The free exciton line E shows no noticeable shift with variations of temperature and laser power density.

A. Free exciton PL emission (E band)

With increasing laser excitation intensity up to 1920 mW/cm^2 we found a broadening of the high-energy side of the free exciton PL line (Fig. 3), which may indicate a manifestation of the fine structure in the exciton spectrum (marked as E_1 and E_2 peaks). The PL features $E_1 = 2.252$ eV and $E_2 = 2.261$ eV can be resolved more clearly in the derivative curve of the PL intensity versus energy (inset in Fig. 3). The PL spectra in Fig. 3 were recorded at T=8 K, which corresponds to the orthorhombic phase of the $CH_3NH_3PbBr_3$ perovskite. In semiconductors with low crystalline symmetry, splitting of the valence band due to "crystal-field splitting" can be observed, resulting in two closely spaced PL lines, or the presence of a small strain may give a similar effect. However, the band structure of hybrid organic-inorganic perovskites differs significantly from the band structure of widely used

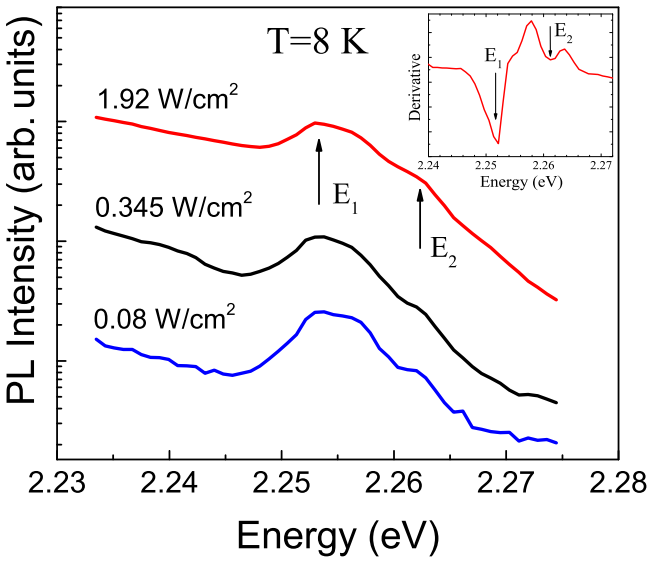

FIG. 3. PL spectra of $MAPbBr_3$ single crystals as a function of energy at $T = 8$ K, recorded for different laser excitation intensities. Inset shows a derivative of intensity versus energy for laser power density 1.92 W/cm^2.

group IV, III-V, and II-VI semiconductors. In perovskites, both the valence band top and the conduction band bottom are twofold degenerate, while the valence band top is fourfold degenerate in III-V and II-VI compounds [27]. Therefore, we assume that the 9 meV E line splitting observed at high laser energies is related to the excited state of the exciton rather than "crystal-field splitting."

It is generally accepted that the excitons generated in the bulk of organic-inorganic perovskites are Wannier-Mott excitons, and they are often described in terms of the hydrogen model [8,28]. Depending on the reduced exciton mass and the dielectric constant, one distinguishes between Wannier-Mott excitons, which extend over many lattice constants and are free to move through the lattice, and Frenkel excitons, which have a radius comparable to the interatomic distance. The spectrum of free Wannier-Mott excitons in bulk crystals is described by a Rydberg series with an effective Rydberg constant given by the reduced effective mass and the dielectric constant. A small dielectric constant and a large effective mass give a localized Frenkel exciton, which is similar to an excited atomic state. These excitons have relatively large binding energies, typically greater than 0.5 eV and they cannot be described by a simple hydrogen model [29]. The existence of Wannier-Mott excitons is suggested by the detection of a giant dielectric constant in the perovskites $MAPbBr_3$ [30,31]. We believe that the E exciton in $MaPbBr_3$ perovskite is a Wannier-Mott exciton, and we can use a hydrogen model. The expression for the energy of the nth exciton level in this model was obtained for isotropic parabolic bands.

In such a model, the energy of the nth excitonic level is given by $E_n = E_g - E_b/n^2$, where E_g is the band gap energy, $E_b = R_0\mu/m_0\epsilon_r^2$ can be treated as an effective Rydberg for the excitons, $R_0 = 13.6$ eV is the Rydberg constant, μ is an exciton reduced mass, and ϵ_r is the relative dielectric constant

of the crystal. If the energies E_1 and E_2 in Fig. 3 are the ground and first excited exciton states, respectively, we obtain the exciton binding energy $E_b = 12$ meV, and the band gap value $E_g = 2.264$ eV. The obtained band gap energy of 2.264 eV agrees well with the values of $E_g = 2.258$–2.292 eV by optical and magnetoabsorption spectroscopy [11–13,16]. Further, we can evaluate the crystal's dielectric constant ϵ_r and excitons' Bohr radius r_n using the relation $r_n = \epsilon_r n^2 R_H m_0/\mu$ (where R_H is the Bohr radius of the hydrogen atom, $n = 1, 2$) and the value of $\mu = 0.117 m_0$ determined in [13]. As a result, we have the values $\epsilon_r = 11.52$, $r_1 = 5.22$ nm, and $r_2 = 20.87$ nm, where r_1 is considered as the bulk Bohr radius of the ground-state exciton.

It should be noted that for low-symmetry systems (anisotropic semiconductors), due to anisotropy of reduced mass or dielectric constant [32], the exciton energy is not determined by the simple equation $E_n = E_g - E_b/n^2$. The applicability of a simple hydrogen-like model for a $MAPbBr_3$ perovskite was based on the following considerations. DFT calculations of the band structure of the archetypical material $MAPbI_3$ show that the conduction and valence bands are relatively isotropic and symmetric, with nondegenerated band edges [33]. In this paper, it is shown that the anisotropy of the effective mass is greatly reduced when the spin-orbit coupling is included, and the masses are similar for all functionals. In Ref. [34] the valence band dispersion of the single crystal $CH_3NH_3PbBr_3$ was measured using ARPES, and intense circular dichroism was observed. The authors state that this dispersion is the result of strong spin-orbit coupling. Furthermore, the exciton effective masses obtained in the simple band structure approach are in good agreement with experimental data from magnetooptical studies for various perovskites [4,13]. Therefore, we believe that the anisotropy in reduced mass in a $MAPbBr_3$ crystal is not so significant. Dielectric studies in $MAPbBr_3$ single crystals [35,36] have shown that in the orthorhombic phase the real part of the dielectric permittivity is practically independent of temperature and there is weak dielectric dispersion and loss. As for the anisotropy of the dielectric constant in this perovskite, there is little data available.

Our value of the exciton binding energy $E_b = 12$ meV turned out to be lower than previously assumed (varying between 25 and 150 meV) [8–10,12–16]. Similar to our data, the values $E_b = 15.33$ meV, $r_1 = 4.38$ nm, $r_2 = 17.53$ nm, and $\epsilon_r = 10.75$ were previously obtained in bulk $MAPbBr_3$ single crystals by recording the reflectance, steady-state, and transient PL spectra of submicron volumes across the crystal [11]. The good agreement with the data obtained on the submicron volumes in $MAPbBr_3$ may indicate a structural perfection of our crystals. A noticeable difference of $E_b = 12$ meV from values estimated by other methods may be due to the fact that in the hydrogen model the exciton binding energy depends on the effective mass of the carriers and the dielectric constant of the crystal. In trihalide perovskites, typical values of the effective mass of the carriers are $0.2 m_0$, which leads to small variations of the exciton reduced mass within 0.09–$0.13 m_0$ [4,13,37] and cannot give a large spread of E_b. However, there is a significant difference between the static and optical dielectric constants in hybrid perovskites [30,31,35,38] which is absent in inorganic semiconductors. An arbitrary choice of the dielectric constant values used in the calculations results in a large scattering of E_b. In addition, the observation of a giant dielectric constant in a $MAPbBr_3$ perovskite [30,31] indicates an exciton binding energy lower than a few tens of meV. The defined by us the value of $\epsilon_r = 11.52$ is an intermediate value between extreme points (between the static and optical dielectric constants). Our measurements of laser intensity-dependent photoluminescence near the optical band edge give a more accurate value for the exciton binding energy, since only one parameter, the exciton reduced mass, was taken from another experiment.

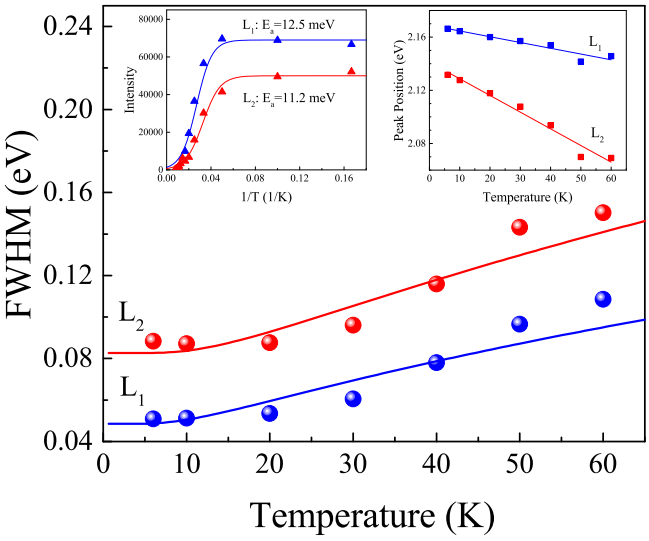

FIG. 4. FWHM of the L_1 and L_2 peaks in $MAPbBr_3$ single crystals as a function of temperature (balls). Solid lines: fitted curves defined as $W(T) = W_0\sqrt{\coth(\hbar\omega_0/2k_BT)}$ with $W_0 = 49$ meV, $\hbar\omega_0 = 2.8$ meV for the L_1 peak, and $W_0 = 83$ meV, $\hbar\omega_0 = 3.7$ meV for the L_2 peak. Inset 1: PL intensity for the L_1 and L_2 peaks (triangles), straight lines are fitted by the equation $I(T) = I_0/(1 + C\exp(-E_a/k_BT)$ with $E_a = 12.5$ meV for the L_1 peak, and $E_a = 11.2$ meV for the L_2 peak. Inset 2 shows the temperature dependence of the L_1 and L_2 peak positions (squares).

B. Wide yellow-light PL emission (L band)

The observed broad yellow-light PL band (L band) was decomposed into two Gaussian peaks, which we named $L_1 = 2.166$ eV and $L_2 = 2.132$ eV lines (see inset in Fig. 1). The intensities of these peaks decreased with increasing temperature from 6 K to 140 K with the activation energies of 12.5 meV and 11.2 meV for L_1 and L_2 peaks, respectively (inset in Fig. 4). The full width of the L_1 or L_2 peak (Fig. 4) significantly exceeded the exciton linewidth, which can be caused by strong electron-phonon coupling and the presence of lattice defects. The appearance of a broad PL band involving deep defects can be illustrated as follows. For a deep acceptor, the hole wave function is localized at one of the bonds and its asymmetric location would cause the atoms to shift from their ideal sites. After recombination of the bound hole with a free electron or electron at a spatially separated donor, the atoms would move to their original sites because all the bonds are restored and equivalent. Atomic relaxation causes lattice vibrations, i.e., emission phonons.

In different recombination processes, the number of emitted phonons is different, resulting in a broad PL band [39]. The temperature dependence of the broadening of the defect PL bands in terms of a configuration coordinate diagram can be written as $W(T) = W_0\sqrt{\coth(\hbar\omega_0/2k_BT)}$, where W is a full width at half maximum (FWHM), and k_B is the Boltzmann constant [39,40]. If $\omega_e = \omega_g = \omega_0$, where ω_e and ω_g are the phonon frequencies for the excited and ground states, respectively, then $W_0 = \hbar\omega_0\sqrt{8\ln 2S} \approx 2.355\hbar\omega_0\sqrt{S}$, where S is the Huang-Rhys factor. Thus, from the temperature-dependent broadening of the L_1 and L_2 bands, the vibrational frequencies $\hbar\omega_0$ and the Huang-Rhys factor S can be determined. The Huang-Rhys factor essentially quantifies the number of phonons emitted during the optical transition and determines the Franck-Condon shift $d_{FC} = S\hbar\omega_0$. For the L_1 peak, the best fit was obtained with values of $W_0 = 49$ meV and $\hbar\omega_0 = 2.8$ meV, and for the L_2 peak with values of $W_0 = 83$ meV and $\hbar\omega_0 = 3.7$ meV (Fig. 4). The Franck-Condon shift and the Huang-Rhys factor for the L_1 band are $d_{FC} = 157$ meV and $S = 56$, and for the L_2 band are $d_{FC} = 333$ meV and $S = 90$. The values of the phonon frequencies obtained in the perovskite $MAPbBr_3$ turned out to be quite small (2.8 meV and 3.7 meV) at large values of the S factor. Similar values of $S = 42$ with phonon energies of 7 meV have already been reported in other wide-gap semiconductors, the inorganic halide perovskites $A_3M_2I_9$ (A=Cs, Rb; M=Bi, Sb) [41]. The authors interpreted these data as a manifestation of strong electron-phonon coupling and self-trapped excitons in the defect perovskites. Raman spectra of the organic-inorganic perovskite $CN_3NH_3PbBr_3$ have revealed small values of the phonon frequencies of 4–6 meV due to lattice vibrations [42]. Therefore, the factor $S = 56$ and the phonon energy of 2.8 meV that we have determined for the L_1 band in the organic-inorganic perovskite $MAPbBr_3$ seem to be quite reasonable.

The high values of the Huang-Rhys factor ($S \gg 10$) usually indicate strong electron-phonon coupling and a deep defect level. Based on the configuration coordinate diagram for deep defects, the position of the zero-phonon line should be at $E_{ZPL} = 2.323$ eV for the L_1 peak, and $E_{ZPL} = 2.465$ eV for the L_2 peak, since $E_{ZPL} = E_{PL} + d_{FC}$. These values of E_{ZPL} exceed the bandgap energy $E_g = 2.264$ eV in the $MAPbBr_3$ crystal, leading to a negative value of the binding energy of the defect ($E_b^{def} = E_g - E_{ZPL}$). Therefore, we assume that the assignment of PL emission bands at energies L_1 and L_2 to deep centers is not suitable. If we assume that the energies L_1 and L_2 are caused by band-to-shallow defect transitions, then the position of the PL peaks of such transitions must satisfy the expression $E_{PL} = E_g - d_{FC} - \Delta$, where Δ is the transition energy of the defect counted from the conduction band minimum (or valence band maximum). In this case, we get the negative values: $\Delta = -0.059$ eV for the L_1 band and $\Delta = -0.201$ eV for the L_2 band, which is incorrect. We have observed similar PL features (two broad PL bands with energy below the free exciton line and phonon energy around 4 meV) in methylammonium lead iodide ($MAPbI_3$) single crystals at low temperatures [43]. We identified the broad PL emissions in $MAPbI_3$ single crystals as donor-acceptor pair recombination and self-trapped exciton recombination. It is natural to assume that $MAPbI_3$ and $MAPbBr_3$ crystals share the same low-temperature PL features, since they differ only in the halogen.

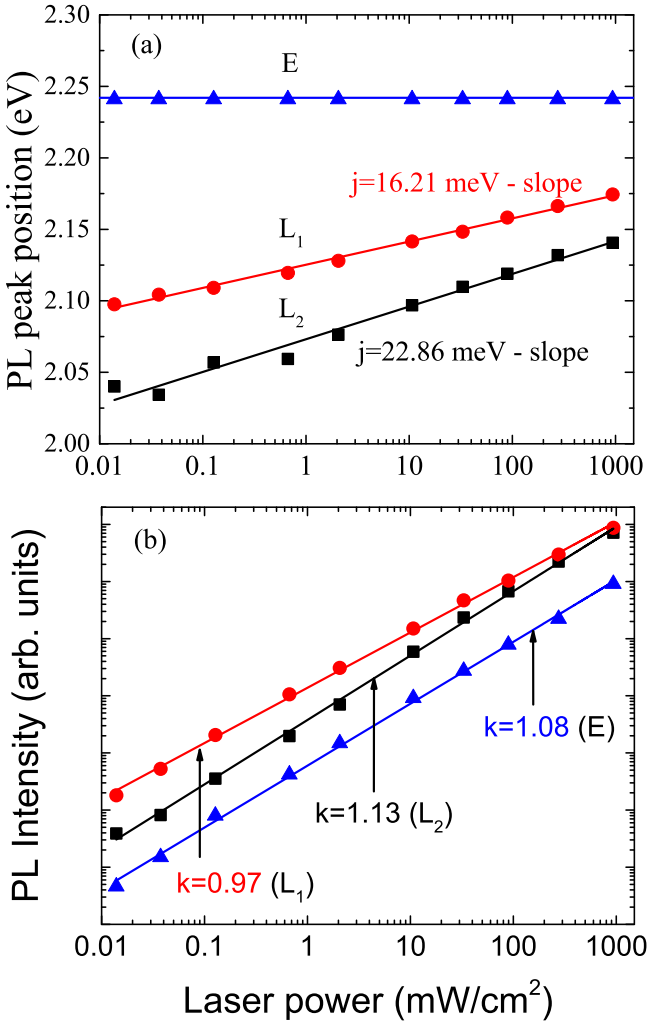

FIG. 5. (a) Laser power density dependence of the E, L_1, and L_2 peak positions (a) and intensities (b) in $MAPbBr_3$ single crystals, $T = 6$ K.

To further investigate the origin of the PL bands at $L_1 = 2.166$ eV and $L_2 = 2.132$ eV, we use the laser power dependent PL. The dependencies of the peak position and integral intensity of the PL bands at $T = 6$ K are shown in Fig. 5. Increasing the laser power induces a different blue shift of the spectral position of the L_1 and L_2 bands: the L_2 line shows a stronger blue shift (slope is 22.86 meV/decade) compared to the L_1 line (slope is 16.21 meV/decade) [Fig. 5(a)]. The dependence of the PL intensity I of the E, L_1, and L_2 bands on the excitation laser power can be described as $I \sim P^k$, where k is a coefficient that can be determined from the gradient of a straight line fitted to a $\log(I) - \log(P)$ scale [Fig. 5(b)]. For excitation laser light exceeding the gap energy, the coefficient k is generally $1 < k < 2$ for the free- and bound-exciton emission, and k is less than one for free-to-bound and donor-acceptor pair (DAP) recombination [25]. Based on our experimental values of $k = 0.97$ for the L_1 peak, $k = 1.08$ for the E peak, and $k = 1.13$ for the L_2 peak, we conclude that the E and L_2 peaks are due to free and bound

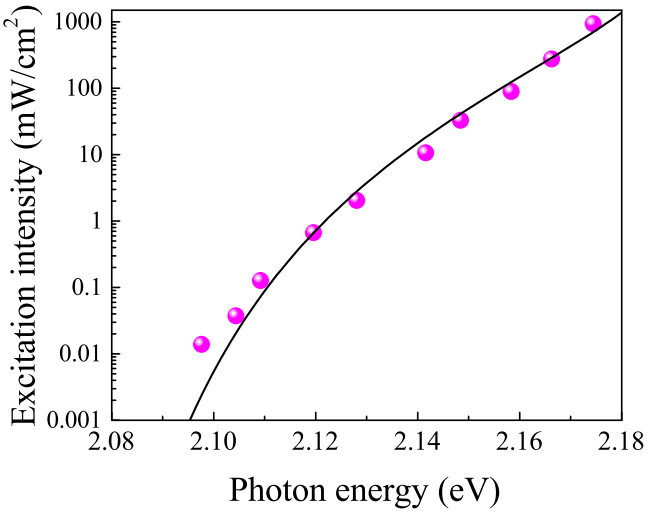

FIG. 6. Laser power density dependence of the L_1 peak positions in $MAPbBr_3$ single crystals (balls), parameters in theoretical fitting (full curve): $D = 1.6 \cdot 10^6$, $h\gamma_B = 2.335$ eV, $h\gamma_\infty = 2.053$ eV.

exciton emission, respectively, and the L_1 band is caused by DAP recombination, since we previously excluded the free-to-bound transition in the model of the configuration coordinate diagram.

For donor-acceptor pair transition, the peak energy is given by [44–46]

$$E_{PL} = E_g - (E_A + E_D) + (e^2/\epsilon r), \tag{1}$$

where E_A and E_D are the acceptor and donor ground-state energies, respectively, r is the acceptor-donor pair distance, and ϵ is the low frequency dielectric constant. The term $(e^2/\epsilon r)$ takes into account the Coulomb attraction between the charged impurities in the final state. As laser excitation increases, the peak position due to DAP recombination is shifted to higher energy and is related to the saturation of recombination of more distant pairs and with decreasing the term $(E_A + E_D)$. In [45] an analytical expression is derived for the dependence of the peak energy of the DAP recombination emission on the excitation intensity J:

$$J = D\frac{(h\gamma_m - h\gamma_\infty)^3}{h\gamma_B + h\gamma_\infty - 2h\gamma_m} \exp\left(-\frac{2(h\gamma_B - h\gamma_\infty)}{h\gamma_m - h\gamma_\infty}\right), \tag{2}$$

where D, $h\gamma_B$, and $h\gamma_\infty$ are the fitting parameters, and $h\gamma_m$ is the measured photon energy. We used the experimental data for the L_1 peak presented in Fig. 5(a) to calculate the parameters appearing in Eq. (2). Figure 6 shows a best-fit curve with the parameters $D = 1.6 \cdot 10^6$, $h\gamma_B = 2.335$ eV, and $h\gamma_\infty = 2.053$ eV. The D parameter includes an arbitrary proportionality factor, and this value is unimportant, more significant are the parameters $h\gamma_\infty = E_g - (E_A + E_D)$ and $E_B = h\gamma_B - h\gamma_\infty$. From the magnitudes of $h\gamma_\infty$ and $h\gamma_B$, we can estimate $(E_A + E_D) = E_g - h\gamma_\infty$, taking $E_g = 2.264$ eV, which gives $(E_A + E_D) = 0.211$ eV and $E_B = 0.282$ eV.

Now, assuming that one of the impurities produces a shallow hydrogen energy level and the other a much deeper one, we have $E_B = e^2/\epsilon R_B$, where R_B is the parameter that determines the overlap of the wave function of the donor and acceptor neutral states [45,46]. With $E_B = 0.282$ eV and $\epsilon = 11.52$ we obtain the value of $R_B = 4.43$ Å. A simple hydrogen model for the shallow acceptor (or donor) level gives $E_A = (13.6/\epsilon^2)(m^*/m_0)$ and $R_B/R_H = \epsilon(m_0/m^*)$, where m^*/m_0 is the relative effective mass at the acceptor and $R_H = 0.53$ Å is the Bohr radius for hydrogen. These equations give $E_A = (13.6/\epsilon)(R_H/R_B)$, and inserting $\epsilon = 11.52$ and $R_B = 4.43$ Å (present work) we have $E_A = 141$ meV, since we have found that $(E_A + E_D) = 0.211$ eV then $E_D = 70$ meV. Using Eq. (2) and $(e^2/\epsilon r) = E_{PL1} - E_g + (E_A + E_D) = 0.113$ eV, we obtain the acceptor-donor pair distance of $r = 11$ Å. A similar value of 10 Å for the average distance between donor and acceptor has been determined in perovskite single crystals $FA_{0.1}MA_{0.9}PbI_3$ for the two vacancies (I-MA vacancy pair) forming a Schottky defect (anion and cation vacancies occurring together) within a unit cell [47]. Density functional theory calculations showed that the dominant defects with low formation energy in $CH_3NH_3PbBr_3$ perovskites create only shallow levels, and the Fermi levels are always pinned by the intrinsic point defects such as V_{Br} (donor) and V_{Pb} (acceptor) [48]. The distance between such a donor and acceptor forming a Schottky defect can be about 11 Å in $MAPbBr_3$ perovskites, since in the low-temperature orthorhombic phase the lattice parameters are equal: a=7.9335 Å, b=11.8301 Å, and c=8.5747 Å [21]. In $MAPbI_3$ single crystals, we have attributed the broad PL line at 1.52 eV to DAP recombination with ionization energies of $E_A = 120$ meV (lead vacancy V_{Pb}^{2-}) and $E_D = 12$ meV (MA interstitial MA_i^+) [43]. The value of $E_A = 120$ meV for the lead vacancy in $MAPbI_3$ agrees well with the present result of $E_A = 141$ meV in $MAPbBr_3$. We suggest that in $MAPbBr_3$ perovskites the DAP transition (L_1 band) is caused by the native defects—lead and bromine vacancies. Note that in organic-inorganic lead halide perovskites, halide vacancies are among the most common point defects [49,50].

The PL emission at 2.132 eV (L_2 peak) was observed in the low-temperature orthorhombic phase up to 130 K. Laser power dependence of the intensity for the L_2 peak is well approximated by the expression $I \sim P^k$ with $k = 1.13$ [Fig. 5(b)], therefore, we believe that the L_2 peak is due to excitons bound to defects or impurities. Large values of Franck-Condon shift ($d_{FC} = 333$ meV) and Huang-Rhys factor ($S = 90$) for the L_2 band indicate a strong electron-phonon coupling, which often leads to the formation of self-trapped excitons (STE). A significant blue shift of the L_2 line with increasing laser power [Fig. 5(a)] may be related to the localization of excitons in traps with several energy levels. As the laser intensity is increased, the higher energy levels of the trap are filled, and the emission line shifts to higher energies. Another feature of the L_2 emission is significant temperature-induced redshift (63 meV in the temperature range 6–60 K, see inset in Fig. 4). It is probably related to the thermal activation of self-trapped excitons and subsequent trapping to lower energy states. The thermal quenching of the L_2 band was fitted with an activation energy 11.2 meV (inset in Fig. 4), and this value corresponds to the self-trapped depth E_{STE}, which is defined as the energy difference between the bottom of the free exciton band and the STE state. The magnitude of 11.2 meV is equal to 130 K, which is why the L_2 band is observed up to 130 K, with further temperature increase as the STE state disappears. In $MAPbI_3$ single crystals, we

found that interstitial iodine I_i^{1-} is likely to be an active trap source with a self-trapped depth E_{STE} of 15 meV [43]. In bromide perovskites, the interstitial bromine with the charge state +1 (Br_i^{1+}) is stable and close to the valence band maximum [51,52]. Since in $MAPbBr_3$ crystals $E_g = 2.264$ eV and L_2 peak energy 2.132 eV is close to band edge, then STE recombination can be caused by interstitial defect Br_i^{1+}.

IV. CONCLUSION

In summary, we have performed in detail near-band-edge study of the temperature and laser power dependent photoluminescence in the orthorhombic phase of single crystal $MAPbBr_3$. We found a sharp PL peak at 2.25 eV and a broad yellow-light emission band centered at about 2.16 eV, which shifted to the blue range with increasing of laser power density. We attributed the peak at 2.25 eV to free exciton recombination, and the broad emission band at 2.16 eV to donor-acceptor pair recombination and self-trapped exciton recombination. The FWHMs of the DAP and STE bands significantly exceeded the exciton linewidth, indicating strong electron-phonon coupling and the presence of lattice defects. Based on the configuration coordinate diagram, we determined the Franck-Condon shift and the Huang-Rhys factor as $d_{FC} = 157$ meV and $S = 56$ for the DAP band, and $d_{FC} = 333$ meV and $S = 90$ for the STE band. From the approximation of the experimental dependence of the peak energy of the DAP recombination on the laser excitation intensity, we obtained the values of the donor and acceptor ionization energies $(E_A + E_D) = 0.211$ meV, and the acceptor-donor pair distance $r = 11$ Å. We assume that in $MAPbBr_3$ perovskites the DAP transition is caused by the native defects—lead and bromine vacancies forming a Schottky defect, STE recombination—by an interstitial defect Br_i^{1+}. The small self-trapped depth E_{STE} of 11.2 meV, estimated from thermal quenching of the STE band, explains why the STE transition is observed only in the low-temperature orthorhombic phase. At high laser power intensity (up to 1920 mW/cm^2), we detected the resolved hydrogen-like Wannier-Mott transitions in the PL spectra with a small exciton binding energy of 12 meV. Applying the hydrogenlike model, we estimated the bulk Bohr radius of the ground-state exciton to be 5.22 nm and the dielectric constant to be 11.52. The lower value of exciton binding energy obtained in $MAPbBr_3$ perovskites compared to other data emphasizes their beneficial properties for photovoltaics due to the more efficient charge separation, and the identification of yellow-light photoluminescence emission can be useful in the design of optoelectronic devices.

ACKNOWLEDGMENTS

This research was carried out within the state assignment No. 122021000039-4 and partially supported by the Ministry of Science and Higher Education of the Russian Federation (through the basic part of the government mandate, Project No. FEUZ-2023-0013 and program of strategic academic leadership "Priority 2030").

[1] A. Kojima, K. Teshima, Y. Shirai, and T. Miyasaka, Organometal halide perovskites as visible-light sensitizers for photovoltaic cells, J. Am. Chem. Soc. **131**, 6050 (2009).

[2] N. J. Jeon, H. Na, E. H. Jung, T.-Y. Yang, Y. G. Lee, G. Kim, H.-W. Shin, S. Il Seok, J. Lee, and J. Seo, A fluorene-terminated hole-transporting material for highly efficient and stable perovskite solar cells, Nature Energy **3**, 682 (2018).

[3] J. S. Manser, J. A. Christians, and P. V. Kamat, Intriguing optoelectronic properties of metal halide perovskites, Chem. Rev. **116**, 12956 (2016).

[4] A. Miyata, A. Mitioglu, P. Plochocka, O. Portugall, J. T.-W. Wang, S. D. Stranks, H. J. Snaith, and R. J. Nicholas, Direct measurement of the exciton binding energy and effective masses for charge carriers in organic-inorganic tri-halide perovskites, Nat. Phys. **11**, 582 (2015).

[5] Q. Dong, Y. Fang, Y. Shao, P. Mulligan, J. Qiu, L. Cao, and J. Huang, Electron-hole diffusion lengths >175 μm in solution-grown $CH_3NH_3PbI_3$ single crystals, Science **347**, 967 (2015).

[6] D. W. deQuilettes, K. Frohna, D. Emin, T. Kirchartz, V. Bulovic, D. S. Ginger, and S. D. Stranks, Charge-carrier recombination in halide perovskites, Chem. Rev. **119**, 11007 (2019).

[7] S. Diyali, M. Manna, S. Mahato, V. Kumar, A. R. Choudhury, B. Biswas, and S. Bhandari, Hybrid lead bromide perovskite single crystals coupled with a zinc (II) complex for white light emission, J. Phys. Chem. Lett. **13**, 10759 (2022).

[8] Y. Jiang, X. Wang, and A. Pan, Properties of excitons and photogenerated charge carriers in metal halide perovskites, Adv. Mater. **31**, 1806671 (2019).

[9] Y. Liu, H. Lu, J. Niu, H. Zhang, S. Lou, C. Gao, Y. Zhan, X. Zhang, Q. Jin, and L. Zheng, Temperature-dependent photoluminescence spectra and decay dynamics of $MAPbBr_3$ and $MAPbI_3$ thin films, AIP Adv. **8**, 095108 (2018).

[10] B. Wenger, P. K. Nayak, X. Wen, S. V. Kesava, N. K. Noel, and H. J. Snaith, Consolidation of the optoelectronic properties of $CH_3NH_3PbBr_3$ perovskite single crystals, Nat. Commun. **8**, 590 (2017).

[11] J. Tilchin, D. H. Dirin, G. I. Maikov, A. Sashchiuk, M. V. Kovalenko, and E. Lifshitz, Hydrogen-like Wannier-Mott excitons in single crystal of methylammonium lead bromide perovskite, ACS Nano **10**, 6363 (2016).

[12] K. Tanaka, T. Takahashi, T. Ban, T. Kondo, K. Uchida, and N. Miura, Comparative study on the excitons in lead-halide-based perovskite-type crystals $CH_3NH_3PbBr_3$ $CH_3NH_3PbI_3$, Solid State Commun. **127**, 619 (2003).

[13] K. Galkowski, A. Mitioglu, A. Miyata, P. Plochocka, O. Portugall, G. E. Eperon, J. T.-W. Wang, T. Stergiopoulos, S. D. Stranks, H. J. Snaith, and R. J. Nicholas, Determination of the exciton binding energy and effective masses for methylammonium and formamidinium lead tri-halide perovskite semiconductors, Energy Environ. Sci. **9**, 962 (2016).

[14] H. C. Woo, J. W. Choi, J. Shin, S.-H. Chin, M. H. Ann, and C.-L. Lee, Temperature-dependent photoluminescence of

$CH_3NH_3PbBr_3$ perovskite quantum dots and bulk counterparts, J. Phys. Chem. Lett. **9**, 4066 (2018).

[15] K. Zheng, Q. Zhu, M. Abdellah, M. E. Messing, W. Zhang, A. Generalov, Y. Niu, L. Ribaud, S. E. Canton, and T. Pullerits, Exciton binding energy and the nature of emissive states in organometal halide perovskites, J. Phys. Chem. Lett. **6**, 2969 (2015).

[16] F. Ruf, M. F. Aygüler, N. Giesbrecht, B. Rendenbach, A. Magin, P. Docampo, H. Kalt, and M. Hetterich, Temperature-dependent studies of exciton binding energy and phase-transition suppression in (Cs, FA, MA)Pb(I, Br)$_3$ perovskites, APL Mater. **7**, 031113 (2019).

[17] M. Li, P. Huang, and H. Zhong, Current understanding of band-edge properties of halide perovskites: Urbach tail, rashba splitting, and exciton binding energy, J. Phys. Chem. Lett. **14**, 1592 (2023).

[18] J. Su, D. P. Chen, and C. T. Lin, Growth of large $CH_3NH_3PbX_3$ (X=I, Br) single crystals in solution, J. Cryst. Growth **422**, 75 (2015).

[19] Y. Cho, H. R. Jung, and W. Jo, Halide perovskite single crystals: growth, characterization, and stability for optoelectronic applications, Nanoscale **14**, 9248 (2022).

[20] A. Jaffe, Y. Lin, C. M. Beavers, J. Voss, W. L. Mao, and H. I. Karunadasa, High-pressure single-crystal structures of 3D lead-halide hybrid perovskites and pressure effects on their electronic and optical properties, ACS Cent. Sci. **2**, 201 (2016).

[21] C. Abia, C. A. López, L. Cañadillas-Delgado, M. T. Fernández-Diaz, and J. A. Alonso, Crystal structure thermal evolution and novel orthorhombic phase of methylammonium lead bromide $CH_3NH_3PbBr_3$, Sci. Rep. **12**, 18647 (2022).

[22] E. H. Bogardus and H. B. Bebb, Bound-exciton, free-exciton, band-acceptor, donor-acceptor, and Auger recombination in GaAs, Phys. Rev. **176**, 993 (1968).

[23] D. Karaiskaj, A. Mascarenhas, J. F. Klem, K. Volz, W. Stolz, M. Adamcyk, and T. Tiedje, Excitons bound to nitrogen pairs in GaAs as seen by photoluminescence of high spectral and spatial resolution, Phys. Rev. B **76**, 125209 (2007).

[24] Y. Zhang, G. M. Dalpian, B. Fluegel, S.-H. Wei, A. Mascarenhas, X.-Y. Huang, J. Li, and L.-W. Wang, Novel approach to tuning the physical properties of organic-inorganic hybrid semiconductors, Phys. Rev. Lett. **96**, 026405 (2006).

[25] T. Schmidt, K. Lischka, and W. Zulehner, Excitation-power dependence of the near-band-edge photoluminescence of semiconductors, Phys. Rev. B **45**, 8989 (1992).

[26] F. Zhang, J. F. Castaneda, S. Chen, W. Wu, M. J. DiNezza, M. Lassise, W. Nie, A. Mohite, Y. Liu, S. Liu, D. Friedman, H. Liu, Q. Chen, Y.-H. Zhang, J. Huang, and Y. Zhang, Comparative studies of optoelectrical properties of prominent PV materials: Halide perovskite, CdTe, and GaAs, Mater. Today **36**, 18 (2020).

[27] M. O. Nestoklon, Tight-binding description of inorganic lead halide perovskites in cubic phase, Comput. Mater. Sci. **196**, 110535 (2021).

[28] M. Baranowski and P. Plochocka, Excitons in metal-halide perovskites, Adv. Energy Mater. **10**, 1903659 (2020).

[29] K. W. Böer and U. W. Pohl, *Semiconductor Physics* (Springer, Cham, 2018), pp. 530–546.

[30] T. Ghosh, S. K. Sharma, and D. Pradhan, Giant dielectric constant and superior photovoltaic property of the mechanochemically synthesized stable $CH_3NH_3PbBr_3$ in a hole transporter-free solar cell, ACS Sustainable Chem. Eng. **8**, 1445 (2020).

[31] M. B. Bechir, A. Almeshal, and M. H. Dhaou, Interpretation of the giant dielectric constant in the single crystal of the $CH_3NH_3PbBr_3$ perovskite, Mater. Res. Bull. **149**, 111723 (2022).

[32] Y. Zhang, A. Mascarenhas, and E. D. Jones, Magnetoexcitons in anisotropic semiconductors, J. Appl. Phys. **83**, 448 (1998).

[33] E. Menéndez-Proupin, P. Palacios, P. Wahnón, and J. C. Conesa, Self-consistent relativistic band structure of the $CH_3NH_3PbI_3$ perovskite, Phys. Rev. B **90**, 045207 (2014).

[34] D. Niesner, M. Wilhelm, I. Levchuk, A. Osvet, S. Shrestha, M. Batentschuk, C. Brabec, and T. Faus, Giant rashba splitting in $CH_3NH_3PbBr_3$ organic-inorganic perovskite, Phys. Rev. Lett. **117**, 126401 (2016).

[35] N. Onoda-Yamamuro, T. Matsuo, and H. Suga, Dielectric study of $CH_3NH_3PbX_3$ (X=Cl, Br, I), J. Phys. Chem. Solids **53**, 935 (1992).

[36] I. Anusca *et al.*, Dielectric response: Answer to many questions in the methylammonium lead halide solar cell absorbers, Adv. Energy Mater. **7**, 1700600 (2017).

[37] Y. Park and D. T. Limmer, Renormalization of excitonic properties by polar phonons, J. Chem. Phys. **157**, 104116 (2022).

[38] M. S. Alias, I. Dursun, M. I. Saidaminov, E. M. Diallo, P. Mishra, T. K. Ng, O. M. Bakr, and B. S. Ooi, Optical constants of $CH_3NH_3PbBr_3$ perovskite thin films measured by spectroscopic ellipsometry, Opt. Express **24**, 16586 (2016).

[39] M. A. Reshchikov and H. Morkoc, Luminescence properties of defects in GaN, J. Appl. Phys. **97**, 061301 (2005).

[40] A. Alkauskas, M. D. McCluskey, and C. G. Van de Walle, Tutorial: Defects in semiconductors -Combining experiment and theory, J. Appl. Phys. **119**, 181101 (2016).

[41] K. M. McCall, C. C. Stoumpos, S. S. Kostina, M. G. Kanatzidis, and B. W. Wessels, Strong electron-phonon coupling and self-trapped excitons in the defect halide perovskites $A_3M_2I_9$ (A=Cs, Rb; M = Bi, Sb), Chem. Mater. **29**, 4129 (2017).

[42] K. Nakada, Y. Matsumoto, Y. Shimoi, K. Yamada, and Y. Furukawa, Temperature-Dependent Evolution of Raman Spectra of Methylammonium Lead Halide Perovskites, $CN_3NH_3PbX_3$ (X = I, Br), Molecules **24**, 626 (2019).

[43] I. V. Zhevstovskikh, N. S. Averkiev, M. N. Sarychev, O. I. Semenova, and O. E. Tereshchenko, Low-temperature luminescence in organic-inorganic lead iodide perovskite single crystals, J. Phys. D: Appl. Phys. **55**, 095105 (2022).

[44] D. G. Thomas, M. Gershenzon, and F. A. Trumbore, Pair spectra and "edge" emission in gallium phosphide, Phys. Rev. **133**, A269 (1964).

[45] E. Zacks and A. Halperin, Dependence of the peak energy of the pair-photoluminescence band on excitation intensity, Phys. Rev. B **6**, 3072 (1972).

[46] N. A. Bogoslovskiy, P. V. Petrov, Y. L. Ivánov, K. D. Tsendin, and N. S. Averkiev, Two components of donor-acceptor recombination in compensated semiconductors: Analytical model of spectra in the presence of electrostatic fluctuations, Phys. Rev. B **98**, 075209 (2018).

[47] A. Francisco-López, B. Charles, M. I. Alonso, M. Garriga, M. T. Weller, and A. R. Goñi, Photoluminescence of

bound-exciton complexes and assignment to shallow defects in methylammonium/formamidinium lead iodide mixed crystals, Adv. Opt. Mater. **9**, 2001969 (2021).

[48] T. Shi, W.-J. Yin, F. Hong, K. Zhu, and Y. Yan, Unipolar self-doping behavior in perovskite $CH_3NH_3PbBr_3$, Appl. Phys. Lett. **106**, 103902 (2015).

[49] J. Ran, B. Wang, Y. Wu, D. Liu, C. M. Perez, A. S. Vasenko, and O. V. Prezhdo, Halide vacancies create no charge traps on lead halide perovskite surfaces but can generate deep traps in the bulk, J. Phys. Chem. Lett. **14**, 6028 (2023).

[50] A. Mannodi-Kanakkithodi, J.-S. Park, A. B. F. Martinson, and M. K. Y. Chan, Defect energetics in pseudo-cubic mixed halide lead perovskites from first-principles, J. Phys. Chem. C **124**, 16729 (2020).

[51] A. Buin, R. Comin, J. Xu, A. H. Ip, and E. H. Sargent, Halide-dependent electronic structure of organolead perovskite materials, Chem. Mater. **27**, 4405 (2015).

[52] D. Shi, V. Adinolff, R. Comin, M. Yuan, E. Alarousu, A. Buin, Y. Chen, S. Hoogland, A. Rothenberger, K. Katsiev, Y. Lasovyj, X. Zhange, P. A. Dowben, O. F. Mohammed, E. H. Sargent, and O. M. Bark, Low trap-state density and long carrier diffusion in organolead trihalide perovskite single crystals, Science **347**, 519 (2015).